Rep. Fac. Sci. Engrg.
Saga Univ
30-1 (2001), 9～16

Reports of the Faculty of Science and Engineering,
Saga University, Vol. 30, No.1, 2001

Passive Control of Exiting Impulsive Wave Caused by Compression Wave from a Tube

By

Toshihiro NAKANO and Shigeru MATSUO

(Received May 1, 2001)

Abstract : An impulsive wave emerges from the open end of a tube as a result of a compression wave traveling down the tube. Such a pulsed jet device has practical applications such as pulse combustion, pulse jet cleaning etc. The geometry of the tube exit affects the strength of the impulsive wave. The effect of flared exit of different geometries on the pressure peak outside the exit is studied by numerical computation after validating computation by experiments.

Nomenclature

a : speed of sound
D : internal diameter of tube
e : total energy per unit volume
P : static pressure
r : distance from exit
t : time
u : velocity component in x-direction
v : velocity component in y-direction
x : longitudinal distance
y : radial distance
γ : ratio of specific heats
ρ : density
θ : azimuth angle
t' : dimensionless time

Superscripts / Subscripts

a : atmosphere
e : exit of tube
m : peak value
s : straight tube exit
* : over pressure

1. Introduction

A compression wave traveling down a tube emerges as an impulsive wave from the open end of the tube. Such a device finds application in pulse combustors[1)]pulse jet filters[2)], pulse jet cleaning[3)] etc. These devices perform better with increasing magnitude of the impulsive wave. This may be achieved by a passive control by modifying of tube exit geometry. To the best of the authors' knowl-

Department of Mechanical Engineering Saga University
1,Honjo-machi, Saga-shi, Saga 840-8502,Japan

edge, there are no studies on augmentation of the impulse wave for practical applications. A flared exit is investigated in the present paper.

The effect of varying the flare length, flare angle and compression wave width on the impulsive wave strength has been found from numerical simulation. Experiments conducted in an open-ended shock tube were utilized for validating the numerical simulation.

2. Test Rig

The tests were done on a shock tube (Fig.1) with a diameter (D) of 66 mm. The total length is about 3.77 m. The length of the driver section is 2.15 m. A sheet of cellophane of thickness 0.03 mm was used as a diaphragm, which was manually ruptured to initiate the wave motion. Driver gas and driven gas are bath air at room temperature.

Pressure transducers flush mounted on the shock tube wall at several stations were used to measure the wave propagating through the tube. A wedge probe with a sharp leading edge with a pressure transducer installed in it was used to measure impulse wave pressure at location r, θ from the duct exit. The wedge was rotatable to measure the wave pressure at different θ directions.

The pressure transducers were calibrated both statically and dynamically prior to each test. The uncertainty in pressure measurement is estimated to be within ± 2 percent.

3. Computational Analysis

The flow fields described in Figure 2 are simulated using a CFD method. Unsteady axisymmetric inviscid conservation equations are solved numerically by assuming a perfect gas (γ=1.4).

$$\frac{\partial U}{\partial t}+\frac{\partial F}{\partial x}+\frac{\partial G}{\partial y}+W=0 \qquad (1)$$

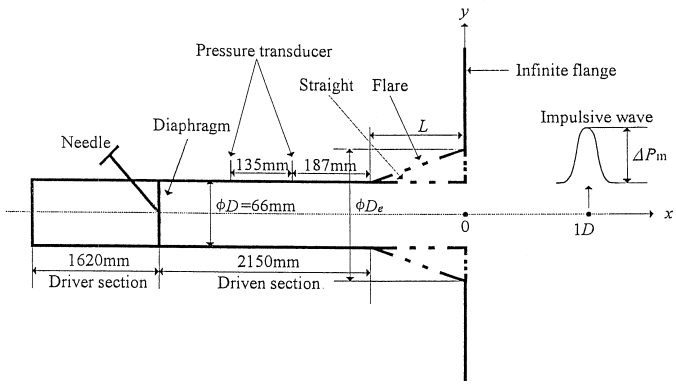

Fig.1 Test set-up

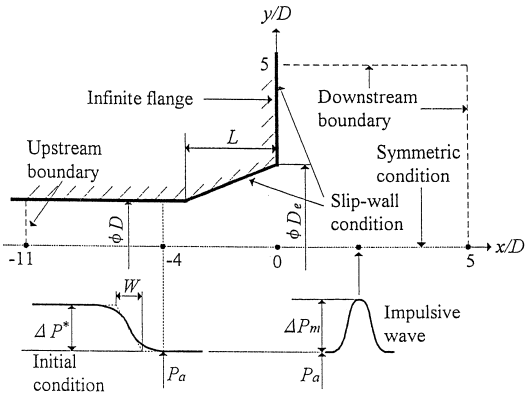

Fig.2 Computational domain and boundary conditions

$$U=\begin{bmatrix}\rho\\ \rho u\\ \rho\nu\\ e\end{bmatrix},F=\begin{bmatrix}\rho u\\ \rho u^2+p\\ \rho u\nu\\ (e+p)\,u\end{bmatrix},G=\begin{bmatrix}\rho u\\ \rho u\nu\\ \rho\nu^2+p\\ (e+p)\nu\end{bmatrix},W=\frac{1}{y}\begin{bmatrix}\nu\rho\\ \rho u\nu\\ \rho\nu^2\\ (e+p)\nu\end{bmatrix}$$

Where x is the longitudinal distance, y the radial distance, ρ the density and, u and ν are the velocity components in x and y directions, respectively. The total energy e per unit volume of the gas is expressed by the sum of the kinetic energy and the internal energy as follow.

$$e=\frac{p}{r-1}+\rho\left(\frac{u^2+\nu^2}{2}\right) \tag{2}$$

Equation (1) is closed by the thermal equation of state of perfect gas, $p=\rho RT$, where T is the temperature. In the computation, equation (1) is rewritten in non-dimensional form by referring the quantities, the pressure, density, etc. to atmospheric condition and the diameter of the shock tube.

$$p'=\frac{p}{p_1},\quad a_1\sqrt{\gamma}u'=\frac{u}{a_1\sqrt{\gamma}},\quad t'=\frac{t}{(D/a_1)\sqrt{\gamma}},\quad x'=\frac{x}{D},\quad y'=\frac{y}{D} \tag{3}$$

The superscript ($'$) indicating the non-dimensional quantities were omitted for the sake of simplicity. The resulting non-dimensional form of Equation (1) was solved numerically using the Harten-Yee TVD scheme[4]. The second order symmetric total variation diminishing (TVD) was incorporated into the operator splitting technique which was suggested by Sod[5].

Figure 2 show the computational domain and boundary conditions used in computation. The initial condition for TVD scheme was taken as,

$$\frac{P}{Pa}=\frac{\Delta P^*}{P_K}\left[\frac{1}{2}-\frac{1}{\pi}\tan^{-1}\left\{\frac{\pi}{W/D}\left(\frac{x}{D}+\frac{22}{3}\right)\right\}\right](x/D\le -4)$$

where

p = Pressure

p_a = atmosphere pressure

Δp^* = over pressure

W = width of compression wave

The inflow and outflow conditions were applied to the upstream and downstream boundaries respectively. Center-line symmetry was used to reduce the computational effort. Slip-wall conditions were applied to the solid wall surfaces. The upstream boundary was located well within the shock tube so as to allow for an expansion wave to travel back upstream.

Cartesian grid was used both inside and outside the tube. Decreasing the grid spacing beyond $\Delta x = \Delta y = D/70$ did not change the solution. Grid spacing of $\Delta x = \Delta y = D/75$ was used in the present computations which ensure that the solutions are independent of grid spacing.

4. Results and Discussion

The measured pressure waveforms at $x/D = -4$, that is, inside the tube and at $r/D = 1$, $\theta = 0°$ outside the tube for the straight tube ($D_e/D = 1.0$) in Fig.3 (a). The waveform which was taken as initial condition for the calculation is also shown. Fig.3 (b) shows the same results for a flared exit of $D_e/D = 1.5$ and $L/D = 1$. The compression wave had on over pressure, Δp^* of 7.2 kPa. We can see that computation predicts the magnitude of the impulse wave accurately, both for straight tube and flared exits. Having thus validated the computation, the magnitude of impulsive wave at different locations ($r/D = 1$ to 3, $\theta = 0°$ to 90°) was computed for different exit geometries ($D_e/D = 1$ to 2.5, $L/D = 1$ to 4)and for wave widths ranging from $w/D = 1$ to $w/D = 3$. The computations were all made for an over-pressure of 20 kPa.

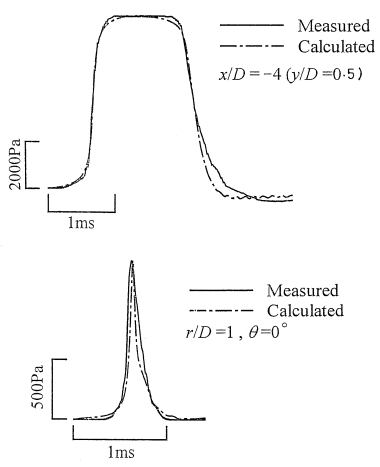

(a) $D_e/D = 1$, $\Delta p^* = 7.2$kpa, $(\partial P/\partial t)_m = 63.196$ kpa/ms

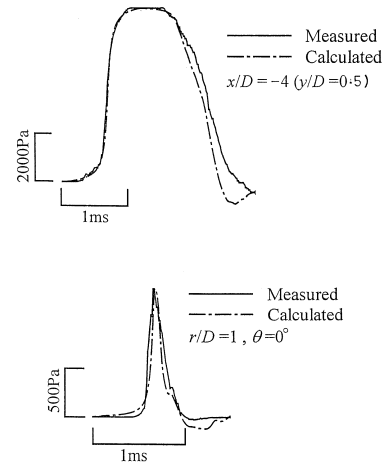

(b) $D_e/D = 1.5$, $\Delta p^* = 7.2$kp, $(\partial P/\partial t)_m = 63.198$kpa/ms, $L/D = 1.0$

Fig.3 Comparison between calculated and measured pressure variation

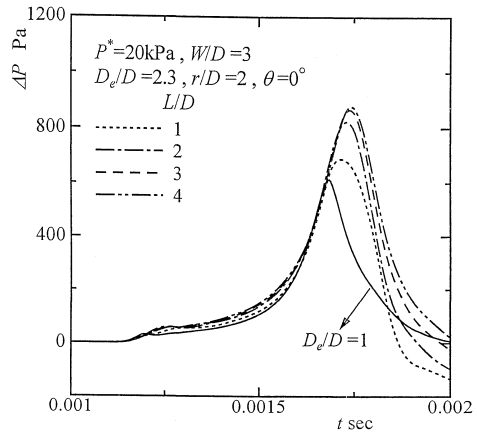

Fig.4 Impulse wave pressure versus time

Fig.4 shows pressure time history at distance $r=2D$ from the exit along the axis $D=0°$ for flare geometry, $D_e/D=2.3$ and L/D varying from 1 to 4. The compression wave width is $3D$. We see that the wave strength keeps on increasing with L/D and is greater than that of straight tube ($D_e/D=1.0$).

The effect of D_e/D on the strength of impulsive wave at a distance of $r=D$ from exit along different azimuth angles $\theta=0$,45 °and 90 °is shown in Fig.5 (a). Similarly Fig.5 (b) and 5 (c) give the results for $r=2D$ and $r=3D$. Wave width $w=2D$ and flare length $L=D$ in all three cases. The results are presented in the form of pressure ratio $\Delta P_m/P_a$, as well as in the form of $\Delta P_m/\Delta P_{ms}$, that is ΔP_m non-dimensionalised by the value for straight tube, ΔP_{ms}. At a distance of $1.0D$ along the axis ($\theta=0°$) (Fig.5 (a)), straight tube gives the highest pressure and flaring does not lead to augmentation, but attenuation of impulsive wave pressure. At azimuthal location $\theta=45°$, peak pressure is maximum for $D_e/D=1.75$ and for $\theta=90°$,it keeps on increasing with D_e/D, up to the maximum value investigated of 2.5.Fig.5 (b) shows that at a distance of $r=2D$, there is augmentation of impulsive wave strength due to flare. At $\theta=0°$, impulsive wave strength becomes maximum at $D_e/D=1.3$ and at $\theta=45°$, it becomes maximum at $D_e/D=1.8$. The strength increases with D_e/D in this case ($r/D=2$) also. Fig.5 (c) shows that impulse wave strength is maximum at the location, $r/D=3$ along $\theta=0°$, for $D_e/D=1.5$ and is maximum at $r=3D$ along $\theta=45°$, for $D_e/D=2.05$. However, at $r=3D$ along$\theta=90°$, wave peak increases with D_e/D to reach a maximum at $D_e/D=1.4$ and then decreases and increases again. In practical applications, impulsive strength along the $\theta=90°$ wall, that is along the wall, is not of great importance.

Finally, Fig.6 shows that effect of flare on impulsive wave peak pressure at a distance of $2D$ downstream from the exit along the axis for three different wave widths. Peak pressure is maximum for flare with $L/D=3$ for all W/D investigated : Fig.6 (a) $W/D=1$, Fig.6 (b) $W/D=2$, Fig.6 (c) $W/D=3$. The wave strength is maximum at $D_e/D=1.39$ for $W/D=1$ and the augmentation due to flare is

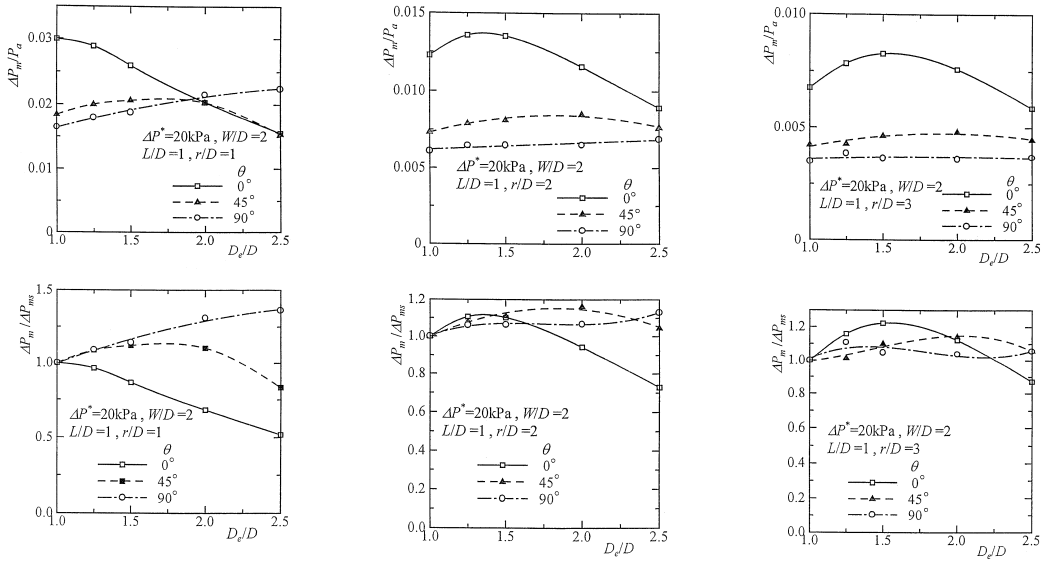

(a)$r/D=1$ (b)$r/D=2$ (c)$W/D=3$

Fig.5 Effect of D_e/D on the strength of impulse wave at different locations

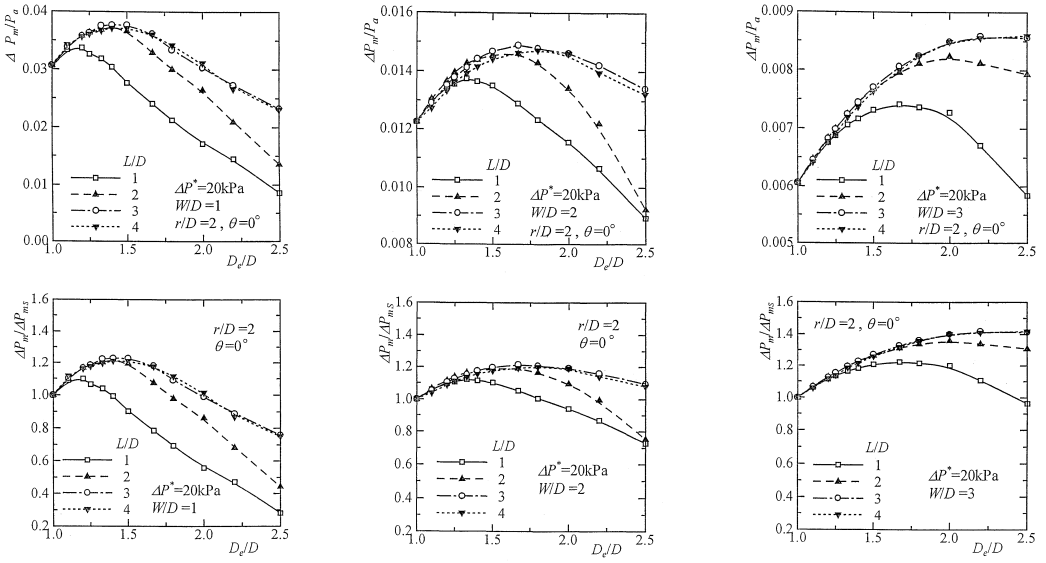

(a) $W/D=1$ (b) $W/D=2$ (c) $W/D=3$

Fig.6 Effect of D_e/D and L/D the strength of impulse wave at the location $r/D=2$, $\theta=0$

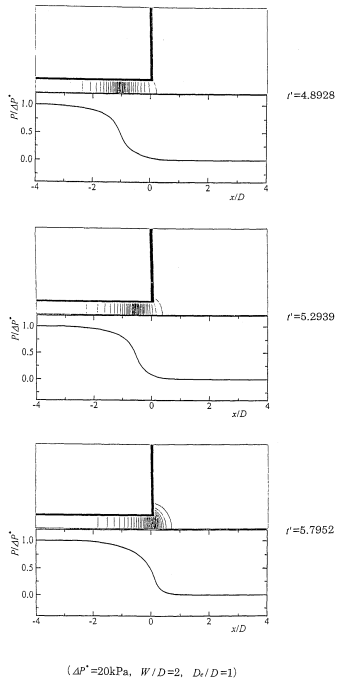

(a) Compression wave propagating inside the tube

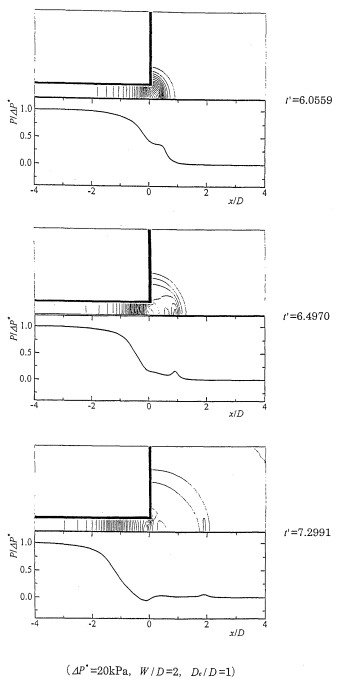

(b) Impulse wave moving outside the tube exit

Fig.7 Iso-bars and axial pressure variation within a straight exit at different times

23%,Fig.6 (a). Augmentation is again 23% for $W/D=2$ for $D_e/D=1.67$, Fig.6 (b) and is as much as 42% for $D_e/D=2.5$ and $W/2=3$.

Computed axial pressure distribution and iso-bars are shown in Fig.7 and 8 for straight tube exit and flared exit respectively. The compression wave propagating down the tube is shown at three different times (non-dimensional) in Fig.7(a). In Fig.7(b), the impulsive wave moving outside the exit is shown. At the last instant of time the wave is seen almost reaching $x=2D$. Fig.8 is for flared exit with $D_e/D=1.5$ and $L/D=1$. The movement of iso-bars gives some idea of how augmentation occurs.

5. Conclusion

The effect of flare at the exit of a tube on the strength of the impulsive wave coming out of it following a compression wave propagating down the tube is investigated by experiment and computation. Experiments were conducted on an open-ended shock tube. Computational analysis was carried out by solving unsteady axisymmetric, inviscid compressible flow equations. An optimum flare geometry exists which maximises the impulsive wave strength at a point 2 tube diameters downstream of the flared exit along the axis. The optimum values of flare length is $3D$. The optimum

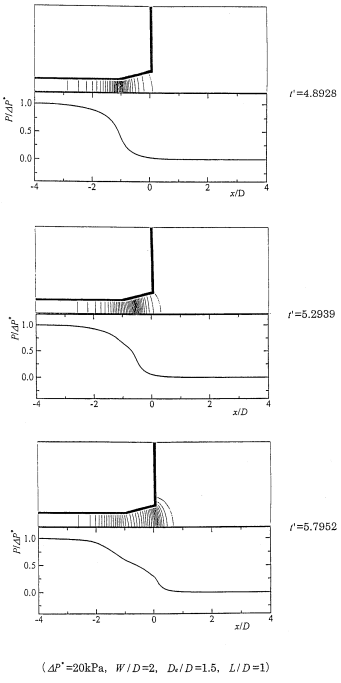

(a) Compression wave propagating inside the tube

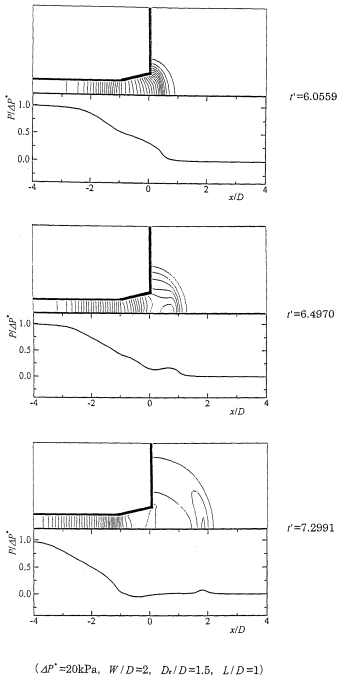

(b) Impulse wave moving outside the tube exit

Fig.8 Iso-bars and axial pressure variation with a flared exit at different times

value of (D_e/D) is 1.39 for compression wave width W/D = 1 and the wave strength was found to be 23% higher than what could be obtained with a straight tube exit. The augmentation is again 23% for a D_e/D of 1.67 for a compression wave width W/D =2. The increase is as high as 42% for D_e/D =2.5 and W/D =3. The is, the optimum diameter ratio D_e/D increases with compression wave width W/D.

References

1. Kentfield, J. A. C., Nonstready, One-Dimensional, Internal, Compressible Flows (Theory and Applications), (1993), Chapter 8, Oxford University Press.
2. Klingel, R and Loffler, F., Dust collection and cleaning efficiency of a pulse Jet fabric filter, Proc. of the Filtration Society, Filtration and Separation, 20, (1983), pp.205-208.
3. Morris, W. J., Cleaning mechanisms in pulse jet fabric filters, Proc. of the Filtration Society, Filtration and Separation, 21, (1984), pp.52-54.
4. Yee, H. C., Upwind and symmetric shock capturing schemes, (1987), NASA TM-89464.
5. Sod, G. A., A numerical study of a converging cylindrical shock. Journal of Fluid Mechanics, 83, (1977), pp.785-794.